Reaction mechanism for natural parity (p, p') transitions in ^{10}B

A. C. Betker,* S. Chang, E. J. Stephenson, A. D. Bacher, S. M. Bowyer, W. A. Franklin, J. Liu, C. Olmer, D. L. Prout, S. P. Wells, S. W. Wissink, and C. Yu
Indiana University Cyclotron Facility, Bloomington, Indiana 47408, USA

R. A. Lindgren, H. Baghaei, and V. Gladyshev
University of Virginia, Charlottesville, Virginia 22901, USA

J. A. Carr, S. K. Yoon, and F. Petrovich**
Florida State University, Tallahassee, Florida 32206, USA

B. L. Clausen
Geoscience Research Institute, Loma Linda University, Loma Linda, California 92350, USA

J. Lisantti
Centenary College of Louisiana, Shreveport, Louisiana 71134, USA
(Received 9 March 2005; published 28 June 2005)

We report angular distribution measurements of the cross section, analyzing power, induced polarization, and all polarization transfer coefficients for the natural parity transitions in ^{10}B$(\vec{p}, \vec{p}')^{10}$B at 197 MeV. All of the transitions closely follow the pattern for spin-1/2 scattering from spin-0, namely $A = P$, $D_{SS'} = D_{LL'}$, and $D_{SL'} = -D_{LS'}$. Small deviations from $D_{NN'} = 1$ reflect spin-flip contributions to these transitions. Distorted wave impulse approximation calculations were generally successful, supporting the use of an empirical effective nucleon-nucleon interaction, the inclusion of channel-coupling in the ground state and the $3^+ \leftrightarrow 4^+$ transition, and the procedure of increasing the $L = 2$ strength of shell-model particle-hole matrix elements to match the collective contribution to these transitions.

DOI: 10.1103/PhysRevC.71.064607 PACS number(s): 24.10.Eq, 24.70.+s, 25.40.Cm, 25.40.Ep

I. INTRODUCTION

Proton inelastic scattering near 200 MeV bombarding energy has been successfully described within a distorted wave impulse approximation (DWIA) framework in which the transition potential is the amplitude for nucleon-nucleon (*NN*) scattering. The quality of agreement with data can be improved if the *NN* interaction is allowed to change with the local nuclear density inside the target. These effects arise, for example, from the Pauli blocking created by the nucleons that surround the struck nucleon, preventing scattering from taking place at low momentum transfer into already occupied intermediate states. A number of authors have investigated such phenomena, and a quantitative picture of Pauli blocking and nuclear binding effects has emerged [1–6].

Pauli blocking and nuclear binding alone do not reproduce the saturation properties of nuclear matter [7]. Better agreement is obtained when relativistic medium effects [8–11] are also included. Pauli, nuclear binding, and relativistic effects have been examined together for (p, p') reactions near 200 MeV [12,13]. It was found that the inclusion of relativistic effects produced better agreement with inelastic scattering analyzing power data but still left some systematic problems, such as the normalization of the cross section, unaddressed.

To have the best possible effective interaction for DWIA calculations, Kelly and coworkers chose to use an empirically adjusted density-dependent interaction that did not have the problems of the theoretically derived interactions. They parametrized the Pauli blocking density dependence and adjusted those parameters, as well as the strength of the interaction, to reproduce a large body of (p, p') data ranging in energy from 100 to 500 MeV on $N = Z$ targets from ^{16}O through ^{40}Ca [14–16]. These data contain measurements of cross section and analyzing power angular distributions for natural parity transitions, most of which are usually regarded as collective. While the form of the density dependence is modeled after Pauli blocking, the adjustment of the model parameters to match data is successful and would thus incorporate relativistic changes as well as other effects present in the nuclear medium such as Δ excitations of the nucleon [17] and many-body forces.

In this paper, we wish to achieve the highest quality theoretical description of the data for ^{10}B$(\vec{p}, \vec{p}')^{10}$B at 197 MeV. We will use the Kelly empirical effective interaction as the best phenomenological model that we have. Its parametrization has been optimized to do an excellent job with many natural parity transitions, although not on targets with the mass this small. While the empirical effective interaction that we will use has been adjusted primarily to reproduce measurements of the cross section and analyzing powers, Liu *et al*. [18] pointed out that the resulting phenomenological effective interaction also describes measurements of polarization transfer. In this

*Presently employed by BITSystems, Inc., Herndon, VA.
**Deceased.

work, we will substantiate this conclusion with a larger body of data.

As part of a study of polarization observables in (p, p') reactions, we have measured a complete set of single- and double-spin observables involving polarized proton beams and the observation of the polarization of the outgoing proton in a suitable polarimeter. Data now exist for the excited states of ^{10}B over a wide range of scattering angles. In this paper, we present the measurements for the natural parity states and discuss what they tell us about the quality of calculations for proton inelastic scattering in the neighborhood of 200 MeV.

The ^{10}B nucleus is deformed and has a 3^+ ground state spin and parity. This introduces the complication that the inelastic scattering, and especially the elastic scattering, may be affected by channel-coupling effects beyond the scope of a one-step distorted wave calculation. Fortunately, a coupled-channel DWIA calculational capability is available [19], and we will apply it to this case since the channel-coupling effects for the elastic channel appear to be large. A similar investigation has been described by Kelly for ^{9}Be [20].

Perhaps the weakest point in the understanding of these transitions lies in our ability to describe the structure appropriately in a particle-hole basis. Various shell-model calculations are now available that can provide us with single-particle matrix elements. When comparing results from several generally accepted interactions, we see little variation among the shell-model predictions. So the question becomes whether these results are adequate to the task of describing what is very likely to be a set of collective transitions. Things are more complicated for ^{10}B since the nonzero spin of the ground state makes it possible to have both non-spin-flip and spin-flip amplitudes contributing to these reactions. Part of our investigation will be to see whether this balance is correctly handled in the shell model.

Problems with the shell-model structure for ^{10}B are evident from its failure to reproduce the form factors measured in inelastic electron scattering. For this analysis, we will attempt to remedy this by increasing the collectivity of the shell-model matrix elements by hand. This means that, whatever else may be wrong, the structure that we use for the (p, p') reaction does reproduce the electron scattering results.

The large number of polarization observables allows us to explore some questions that cannot be addressed with just measurements of cross section and analyzing power alone. Liu [18] and Flanders [21] have pointed out that when the transitions are collective, the polarization transfer measurements often show an approximate adherence to the relationships that exist for spin-1/2 scattering from a spin-0 target with no parity change. The degree to which these relationships hold can be arranged into a hierarchy. The quality of the agreement, or lack of it, thus becomes a measure of the collective nature of the transitions. One observable in particular, $D_{NN'}$, would remain equal to 1 were it not for the presence of spin flip. Thus the polarization transfer measurements, along with the magnetic electron scattering, can become a special test of the description of the spin-flip amplitudes.

In Sec. II, we will review the experimental considerations that lie behind these measurements. Section III will present the analysis and conclusions.

II. EXPERIMENTAL CONSIDERATIONS

The measurements reported in this paper were performed at the Indiana University Cyclotron Facility using the high-resolution K600 spectrometer with its focal plane polarimeter. The polarized proton beam from the cyclotrons was accelerated to 197 MeV. Data on the transition to the second excited (0^+) state at 1.74 MeV in ^{10}B were published earlier [22]. These data included the cross section σ, analyzing power A, induced polarization P, and normal component polarization transfer coefficient $D_{NN'}$.

The polarized proton beam was produced in an atomic beam polarized ion source [23]. The spin direction of the beam was reversed every 20 s by alternating operation between the strong and weak RF transition units. The polarization was first measured following acceleration in the injector cyclotron to an energy of about 15 MeV. There the beam was occasionally interrupted by the insertion of a helium gas cell and Faraday cup assembly into the path of the beam. Protons scattered to the left and right at $\theta_{\rm lab} = 112^\circ$ from the helium went into plastic scintillation detectors with thin reflective front windows. The analyzing power at this angle is larger than 0.99 [24]. This measurement mainly provided a separate determination of the polarization from each RF transition unit so that corrections could be made in the analysis for unequal polarizations in the two spin directions from the polarized ion source. This required a correction based on a separate measurement of the instrumental left-right asymmetry by running this polarimeter with the atomic beam valve on the polarized ion source closed. The much weaker beam that was accelerated to the polarimeter arose only from the molecular background in the polarized ion source and was therefore unpolarized. Corrections were also made to the instrumental asymmetry for calculated differences in the transmission of the two allowed hyperfine states through the atomic beam source. The polarization difference between the forward and reversed directions was typically small, $p_+ - p_- \leqslant 0.006 \pm 0.006$.

For the measurement of polarization transfer coefficients using a beam with the spin aligned in the horizontal plane (the reaction plane for the K600 spectrometer system), it is sufficient to precess the beam after acceleration in the main stage cyclotron. This was achieved by two superconducting solenoids located on either side of a 45° energy analysis magnet located in the beam transport line. The data were taken with three different spin orientations located roughly 60° apart in order to provide an internal consistency check. The 45° bending magnet rendered the effects of the two solenoids nearly orthogonal with regard to the direction of final polarization. This spin precession scheme allowed corrections to compensate for polarization directions at extraction from the cyclotron that were not vertical. The spin orientation on target was calculated from the known bending angles of the magnet system between the two solenoids and in the beam line to the K600 target [25].

The polarization of the precessed beam was measured using two polarimeters, one located just after each of the two precession solenoids. These polarimeters observed $p + d$ elastic scattering from a CD_2 foil target whose thickness was varied between 0.2 and 1.2 mg/cm^2 depending on the beam current and count rate needed. The scattering angle was determined by a collimated stopping scintillator that observed the recoil deuteron at $\theta_{\rm lab} = 42.6^\circ$. The scattered protons were observed in coincidence in a passing scintillator 0.64 cm thick. Elastic events were selected on the basis of detector pulse height and the relative time of flight to the detectors. The analyzing power was calibrated against proton scattering from carbon [26]. The analyzing power value used for this analysis at 197 MeV was 0.507 ± 0.005. Beam polarization measurements were made concurrently with data taking at the K600 spectrometer.

The targets were made from a pressed powder of the separated ^{10}B isotope enriched to better than 99% purity. The main contaminants were ^{11}B and ^{12}C. Avoiding contaminant peaks caused the original plan of polarization transfer measurements every 10° in the laboratory to be altered so that measurements were made at 20°, 31°, 40°, 48°, and 60°. After passing through the target, the beam continued on into a Faraday cup that was recessed to reduce the loss of secondary electrons. The current from this cup was integrated during the course of all of the measurements.

Scattered protons from the target were analyzed by the a horizontal-bend K600 magnetic spectrometer system consisting of a vertically focusing entrance quadrupole magnet and two separately adjustable dipole magnets with edge focusing. Hexapole correction coils were also used. The smaller angle measurements used a slit with a 1° polar angle acceptance and a solid angle of 0.64 msr. Larger angle measurements used a 4° acceptance with a solid angle of 2.60 msr.

The resolution of the K600 spectrometer was based on an image created by a pair of beam-defining slits located ahead of a 130° analyzing magnet system that dispersed the beam on target. The opening of these slits was varied depending on the desired transmission and resolution. The width of the image at the spectrometer focal plane was corrected for a number of optical effects in order to obtain the best resolution. The kinematic displacement of the horizontal (bend plane) focus ahead or behind the focal plane detectors was corrected using a triangular coil located inside the dipole magnet. A significant variation in the scattered particle energy across the spectrometer acceptance (kinematic defocusing) required that the strength of the quadrupole triplet between the analysis magnet and the target be reduced to move the beam focus downstream. Matching the dispersion of the spectrometer dipole to the dispersion of the beam on target required adjusting the horizontal magnification of the last quadrupole triplet by changing the ratio of the currents in the first and last magnets of the set. The angle information available from the focal plane detectors was used to improve resolution to take out additional optical aberrations in the data replay. The resulting resolution varied with scattering angle and was typically less than 100 keV.

The positions and angles of protons passing through the K600 focal plane were measured with a pair of x and y wire chambers. The wire chambers ran with a half-and-half mixture of argon and isobutane. The horizontal (focal) plane measurements used the vertical-drift technique described by Bertozzi *et al.* [27] while the vertical measurements used the technique described by Walenta *et al.* [28]. Triggering and particle identification were provided by a series of two passing scintillators. In polarimeter mode, the second of these was situated directly in front of the carbon analyzer target, which was mounted to be perpendicular to the focal plane proton trajectories. The polarimeter consisted of a thick carbon analyzing target, two sets of x-y proportional chambers for tracking, and two scintillators whose pulse heights were used to select events that scattered elastically in the carbon analyzer target. The carbon analyzer was 5.1 cm thick with a density of 1.79 g/cm^3. The two scintillators were 0.64 and 7.62 cm thick. The first of these scintillators was included in the event trigger when polarization transfer measurements were in progress. Secondary levels of the event trigger checked that there was a good signal in the focal plane wire chambers and that the proton had scattered beyond some minimum angle ($\sim 4^\circ$) in the carbon analyzer. This second requirement eliminated a large fraction of the events that were not useful for a polarization transfer measurement. Unfortunately, this selection, which was based on horizontal plane angles, could not be used with the wide spectrometer entrance slit associated with the largest angle measurements.

The acceptance of an event as useful required that it have the correct energy loss in all scintillators. The correct energy deposition in the last two polarimeter scintillators was calculated on an event-by-event basis using the scattering angle in the analyzer and the assumption that the scattering there was elastic.

To obtain information on both the sideways and longitudinal outgoing polarization components, measurements were made with the focal plane detectors and polarimeter at two locations behind the spectrometer. For these two setups, the ratio of the currents in the two K600 dipoles was changed so that the bending angle of the protons was different by about 22°. The absolute bending angle was measured for each setup geometrically.

The analyzing power of the carbon polarimeter target was a function of energy, and thus it changed across the angular distributions reported here. It was calibrated at a number of energies by using protons elastically scattered from carbon at an angle where the analyzing power crossed through zero (close to 24°). At this angle, the magnitude of the polarization remains fixed in the scattering, and a set of in-plane polarization transfer measurements will yield enough information to deduce the analyzing power. This compared well with the analyzing power deduced for vertical polarization, which is transmitted unchanged through the scattering. The analyzing power varied from 0.40 to 0.53 for the measurements reported here.

III. ANALYSIS

In our theoretical description of the (p, p') reaction, we will constrain as much as possible the ingredients in the calculation

then evaluate the results. This presents two issues for special consideration.

First, the presence of a nonvanishing ground state spin allows for spin-flip contributions to the transition. Thus, we need a more general description of the transition than was used for many of the states previously considered with the Kelly empirical interaction [16]. Rather than use an empirical fit to longitudinal electron scattering to define the transition density, we turned to an expansion in terms of particle and hole shell-model orbitals, in particular $p_{3/2}$ and $p_{1/2}$. This gives us the flexibility to describe both non-spin-flip and spin-flip amplitudes. Because of the large number of matrix elements now involved, we cannot determine them all from the transition form factor data. So we begin with estimates from a shell model. But such matrix elements underestimate the strength of the collective ($L = 2$) part of the transition. So we will adjust this component to obtain agreement with the scale of the (e, e') electric and magnetic form factors.

Second, the ground state of ^{10}B is deformed and its rotation easily couples into the scattering process. So we will include two-way channel coupling to the 4^+ excited state at 6.02 MeV and $L = 2$ self-coupling for the ground state. Since this has a large effect on the elastic scattering observables, we will need to adjust the optical potential for a best fit in the presence of the channel coupling.

We will use the empirical effective interaction without further adjustment. With all of these ingredients in place (distorted waves, interaction, and structure) and constrained by other data, we will make calculations for the natural parity transitions in ^{10}B and evaluate the results. The 4^+ state at 6.02 MeV will be considered first because of its large cross section and highly collective nature. There is also some $L = 2$ strength leading to lower-excitation natural parity states with almost an order of magnitude smaller cross section. These transitions will be considered last.

A. Transition form factors

In the DWIA calculations to be described later, we will be using microscopic form factors made of particle-hole amplitudes to describe the structure for the transitions to the inelastic states and the rotational coupling present in the elastic scattering. In all cases, there are measurements of longitudinal and transverse electron scattering form factors that are sensitive to the same structure components. Since the electron scattering offers the advantage of a known probe, these data can be used as one check on the correctness of the structure amplitudes. Unfortunately, each electron scattering form factor contains contributions from a number of possible particle-hole combinations, and it is not possible to separately determine each one from a comparison to the (e, e') data. So some additional information is needed. One source for the individual coefficients for each particle-hole component would be shell-model calculations. However, we find that these calculations do not provide satisfactory agreement with the (e, e') data, and we need a strategy for making improvements. One way to proceed is to note that shell-model calculations often fail to describe the collectivity of simple, natural parity states since this is not a natural degree of freedom within the model. So we will adopt the scheme of increasing the size of the amplitudes with the correct angular momentum transfer for a collective transition until the size of the total amplitude agrees with the electron scattering data.

Since the shell model provides only particle-hole matrix elements and we need wave functions for the DWIA transition density, we must also choose a radial form for the wave function. This allows additional degrees of freedom in matching the (e, e') data. For this purpose, we will be using harmonic oscillator wave functions where the only adjustable parameter is the radius. Between this and the changes to the size of the collective amplitudes, we have enough latitude in making adjustments to match the electron data. It is important to realize that these changes to the shell-model matrix elements do not guarantee that we have a correct description of the transition. The DWIA calculations are sensitive to the size of each component since it has a unique spin coupling, so whatever problems remain with the matrix elements may be reflected in poorer agreement with the proton inelastic data.

Transitions from the ground state to the natural parity states of ^{10}B have been observed in inelastic electron scattering, and a paper by Cichocki *et al.* [29] reports measurements of the longitudinal and transverse form factors. These new data extend earlier measurements that presented only the elastic data [30], or concentrated on the transverse form factors with an emphasis on unnatural parity excitations [31].

A set of single particle-hole amplitudes has been compiled for transitions in ^{10}B by Lee and Kurath [32] based on the (8–16)POT interaction of Cohen and Kurath [33]. This interaction involves only rearrangements and excitations within the $1p$ shell. Since the lower of these two shells, the $1p_{3/2}$, is not filled for ^{10}B, this space should account for the most important pieces of the transition densities to low-excitation states. Calculations within a larger shell-model basis [34] that included $1s$, $2s$ and $1d$ shells and a newer interaction [35] did not reveal any significant changes in the individual particle-hole amplitudes from the earlier Lee and Kurath results. In particular, there were no new amplitudes whose contributions to the transition densities were more than a few percent. Given that we would change these amplitudes later by even larger amounts in order to match the inelastic electron scattering data, we decided to begin with the Lee and Kurath values, which involved only the $p_{3/2}$ and $p_{1/2}$ orbitals.

Calculations of the electron scattering form factors were made with the program LEA [19]. Harmonic oscillator forms scaled by a single length parameter b described each particle and hole wave function. Center-of-mass corrections were included.

Calculations based just on the Lee and Kurath amplitudes underestimate the inelastic electron scattering form factors typically by as much as a factor of 2. We interpreted this to mean that the transitions in ^{10}B have more collective character than is present in the shell model. Most of the collective excitation in this nucleus proceeds through $L = 2$ transfer. So to model this collectivity, we scaled upward the $L = 2$ components of the particle-hole amplitudes. This involved a transformation of the shell-model matrix elements from the *jj*

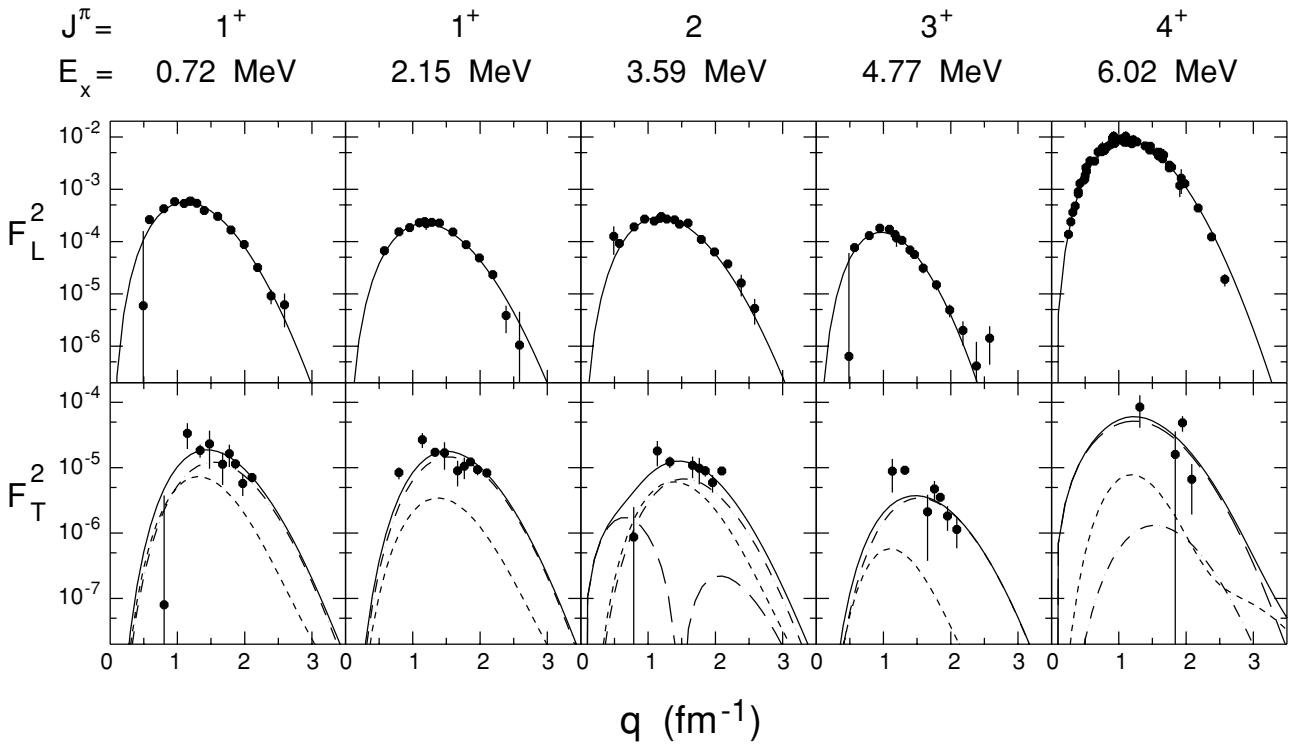

FIG. 1. Measurements of the longitudinal and transverse form factors for five transitions in ^{10}B from Ref. [29]. Each is labeled with spin, parity, and excitation energy. Solid lines indicate the total form factor. Contributions for different ΔJ are indicated by long dash lines for $M1$, short dash lines for $E2$, and dot-dash lines for $M3$.

representation of Lee and Kurath to the LS representation, a rescaling of the $L = 2$ terms, and a transformation back again. To improve agreement with the q dependence of the electron data, we also adjusted the harmonic oscillator parameter b. The final results are shown in Fig. 1 for the inelastic natural parity transitions in ^{10}B.

For these transitions, the dominant contribution to the longitudinal form factor F_T^2 comes from $\Delta J = 2$ ($C2$) as shown by the solid lines in the upper panels. In each case, the data cover a wide enough span in momentum transfer to determine a value for b rather precisely. This is not the case for the transverse form factor. For most of the transitions, only a rough normalization is possible. In most of these cases, we used a value for b in the $\Delta J = 3$ part of the calculations that matched the more extensive measurements for the $3^+ \rightarrow 0^+$ transition at 1.74 MeV [31]. This is shown by the dot-dash curves. The $M1$ contribution (long dash) was large only for the transition to the 4^+ state at 6.02 MeV, and a rough value of the $\Delta J = 1$ b parameter was obtained there; the same value was used for the $M1$ part of the transition to the 2^+ state at 3.59 MeV. The $E2$ contribution (short dash) to the transverse form factor was calculated with the parameters found for the $C2$ longitudinal form factor. Because of the poor internal consistency of some of these measurements, we chose a normalization that matched the average size of the data rather than one that minimized the chi square. Table I contains the harmonic oscillator parameter for each ΔJ component of the transition density. It also includes the ratio by which the $L = 2$ amplitudes were increased. In the case of most $\Delta J = 2$ terms, this adjustment was applied only to the $L = 2$ part, which is indicated by an asterisk in the table. Table II gives the final values of the particle-hole amplitudes as used in our

TABLE I. Form factor parameters. Each entry contains b and R, the rescaling ratio.

State (MeV)	g.s.		0.72		2.15		3.59		4.77		6.02	
J^π	3^+		1^+		1^+		2^+		3^+		4^+	
ΔJ	b	R	b	R	b	R	b	R	b	R	b	R
1	1.45	1.0					1.5	1.0	1.85	1.0	1.51	1.7
2	1.75	1.79	1.75	1.1*	1.67	1.6*	1.67	1.0	2.08	0.6*	1.77	1.68*
3	1.61	1.0	1.53	1.8	1.53	1.0	1.53	4.0	1.53	0.7	1.53	1.0

*Adjusted value; see text for explanation.

TABLE II. Structure coefficients scaled to Raynal Z convention.

State (MeV)	g.s.	0.72	2.15	3.59	4.77	6.02
J^π	3^+	1^+	1^+	2^+	3^+	4^+
$\Delta l = 1$						
$(1p_{3/2},1p_{3/2}^{-1})$	0.4833			−0.0057	0.0028	−0.0646
$(1p_{3/2},1p_{1/2}^{-1})$	0.0878			0.0827	0.0362	−0.1321
$(1p_{1/2},1p_{3/2}^{-1})$	−0.0878			−0.0855	0.0251	0.0
$(1p_{1/2},1p_{1/2}^{-1})$	−0.1159			−0.0170	−0.0100	−0.3150
$\Delta l = 2$						
$(1p_{3/2},1p_{3/2}^{-1})$	−0.3553	−0.837	0.1342	0.0183	−0.0870	0.1817
$(1p_{3/2},1p_{1/2}^{-1})$	−0.3498	0.0335	−0.0652	−0.0199	0.0665	0.2442
$(1p_{1/2},1p_{3/2}^{-1})$	0.3498	0.2015	−0.0906	−0.1842	−0.1451	−0.5552
$\Delta l = 3$						
$(1p_{3/2},1p_{3/2}^{-1})$	0.0500	−0.1970	−0.2160	0.1468	0.1048	−0.0647

calculation. For the transition to the 3^+ state at 4.77 MeV, it is also possible to obtain a $\Delta J = 0$ component. This component was small and not visible on the scale of Fig. 1, so it was omitted from Tables I and II.

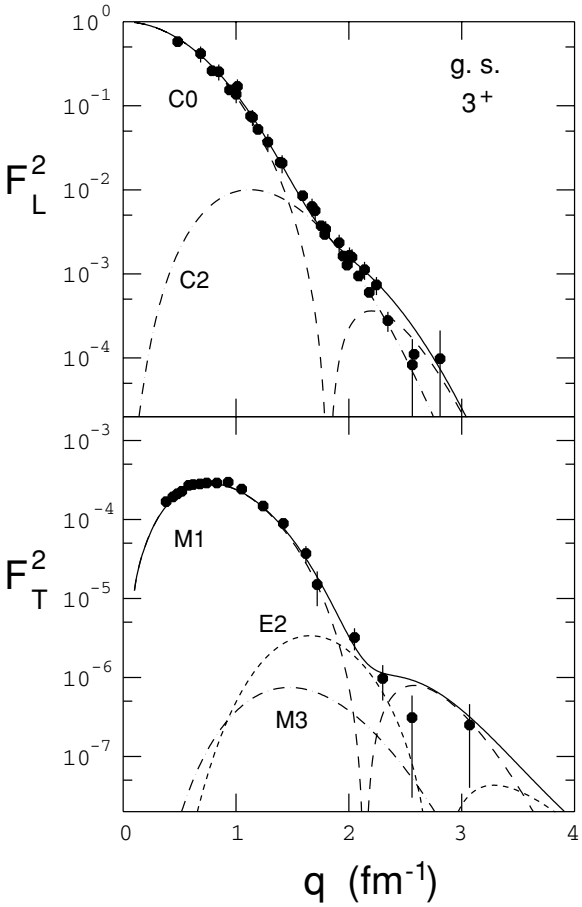

FIG. 2. Measurements of the longitudinal and transverse form factors for scattering from the ground state in ^{10}B from Refs. [29–31]. Solid lines indicate the total form factor; broken lines, contributions for different ΔJ.

Figure 2 shows the transition densities for elastic scattering. Here there is a large $\Delta J = 0$ component that arises from scattering from the nuclear charge distribution. In the (p, p') calculations, this component is represented by the optical potential, which will be adjusted for a best representation of the elastic proton scattering data. For the comparison in Fig. 2, the $\Delta J = 0$ component is given by a harmonic oscillator wave function with $b = 1.65$ fm, including corrections for the center-of-mass motion and the form factor of the proton. This serves to set the scale against which the size of the quadrupole term is estimated. Because only a short range in momentum transfer is available where the quadrupole term dominates, the harmonic oscillator parameter and normalization are not uniquely determined. Following the work of Lewis [36], we have simply increased the $\Delta J = 2$ part by a factor of 1.79. The transverse electron scattering is well matched using the Lee and Kurath amplitudes in their original form.

B. Elastic proton scattering

For the calculation of inelastic proton scattering, it is important to have distortions that describe well at least the low momentum transfer data for elastic scattering. Inelastic scattering that proceeds through the effective *NN* interaction has a large scattering amplitude across a large momentum transfer range. At the same time, the distortions have amplitudes that fall quickly with momentum transfer. Thus, for the large momentum transfer regions explored in this experiment, the dominant contributions pair a large momentum transfer in the *NN* interaction together with a small momentum transfer in the distorted waves.

Typical reproductions of elastic scattering usually weigh the data rather evenly across momentum transfer and thus may sacrifice a high-quality fit at small scattering angles to obtain a more generally satisfactory description across the full angular distribution. For ^{10}B, this problem is especially severe since the 3^+ spin of the ground state makes possible a large quadrupole coupling through a reorientation of the target spin direction. This can be seen as the large $C2$ component in Fig. 2. Such

TABLE III. Optical model parameters (strengths in MeV; lengths in fm).

Term	V_i	r_i	a_i
Real central	−8.9951	1.481	0.5808
Real Gaussian central	9.0615	0.5378	0.8549
Volume imaginary	−28.0739	0.8582	0.685
Real spin orbit	−3.862	0.9323	0.644
Imaginary spin orbit	0.65145	0.951	0.705

contributions are beyond the scope of a simple optical model calculation containing only central and spin-orbit terms. Any attempt to address the elastic scattering data with only optical model techniques would lead to significant problems with the quality of the agreement to any particular portion of the data.

In a similar study of ^{9}Be [20], these issues were addressed through the inclusion of microscopic channel coupling. We took a similar approach, including $M1$, $C2$, $E2$, and $M3$ components for the ground state as well as the excitation of the 4^{+} state at 6.02 MeV, by far the largest discrete collective state in ^{10}B. The expectation was that these additional components would help agreement with the cross section and spin dependence at larger momentum transfer, thus freeing the optical potential to describe well the scattering at small momentum transfer.

Based on the experience with elastic scattering from nuclei in this mass region [36,37], we chose an optical potential with a Gaussian repulsive core in the real, central component. This potential is

$$V(r) = V_{\rm Coul}(r) + V_C f_V(r) + V_G g(r) + iW f_W(r) + 2\left[V_{\rm SL}\frac{1}{r}\frac{d}{dr}f_{\rm SOR}(r) + W_{\rm SL}\frac{1}{r}\frac{d}{dr}f_{\rm SOI}(r)\right]\vec{L}\cdot\vec{\sigma}$$

where

$$f_i(r) = 1/\{1+\exp[(r - r_i A^{1/3})/a_i]\},$$
$$g(r) = \exp\left[-\left(\frac{r - r_G A^{1/3}}{a_G}\right)^2\right],$$

and $V_{\rm Coul}(r)$ is the Coulomb potential generated by a uniformly charged sphere of radius $r = 1.46$ fm. The optical potential parameters were varied to reproduce a set of fictitious data. These were generated from the real cross-section data by subtracting the difference between the coupled channel and the optical model calculation. Analyzing power data out through 25° were also included, since this angle range is dominated by the optical model contribution. The new optical potential was then placed in the coupled-channel calculation to generate a new cross-section difference, and the process iterated. The optical model program used for this search was CUPID [38].

The final optical model parameters are given in Table III. The resulting cross section and analyzing power are given in Fig. 3 by the solid curves. The dashed curves show the contribution from the optical model alone. Beyond about 25°, the channel coupling contributes significantly to the cross section, diminishing the oscillatory behavior in the analyzing power inside 60°. Even with the good description of the electron data for elastic electron scattering, we still appear to be far from a completely satisfactory description of the analyzing power. A similar result was reported for ^{9}Be by Kelly [20].

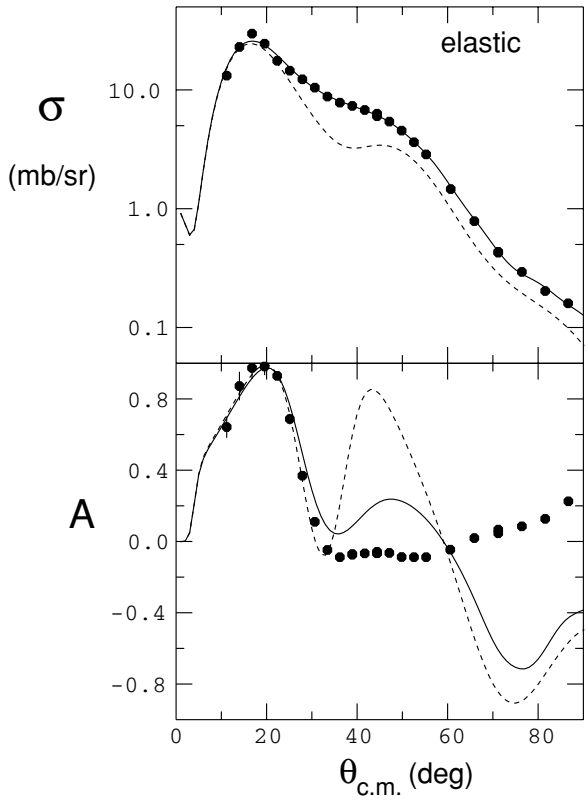

FIG. 3. Measurements of the cross section (ratio to Rutherford) and analyzing power for elastic proton scattering from ^{10}B. Solid lines represent the coupled-channel calculation; dashed lines, the optical model component only.

Figure 4 shows a prediction for the $D_{NN'}$ polarization transfer in elastic scattering, which should directly check

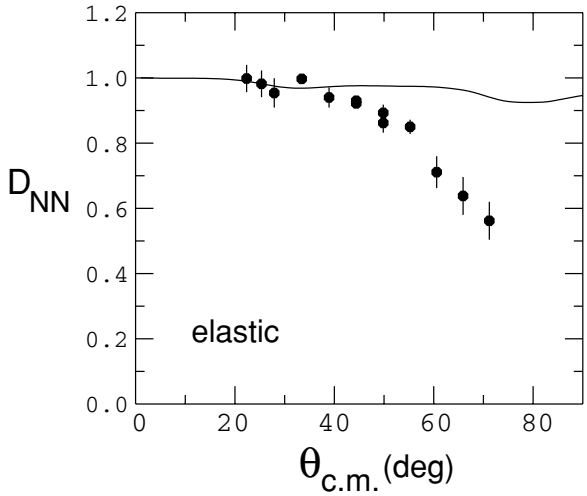

FIG. 4. Measurements of the polarization transfer coefficient $D_{NN'}$ for elastic proton scattering from ^{10}B. Solid line represents the coupled-channel calculation.

the spin-flip contributions coming from the $M1$ and $M3$ components shown in Fig. 2. The coupled-channel prediction is well above these data for almost all of the angles covered, indicating that it contains only a tiny fraction of the spin-flip strength it appears to need.

In the forward angle region, these calculations appear to work well, and that is the region most crucial for a good test of the inelastic scattering calculations. It is clear that there are contributions missing from the elastic scattering that increase the spin-flip and dampen the angular oscillations in the analyzing power.

C. Effective interaction

Inelastic scattering to natural parity, collective states proceeds predominantly through the central and spin-orbit parts of the effective isoscalar NN interaction. Inside the nuclear medium, these parts are the most sensitive to density-dependent changes. The Pauli blocking part suppresses scattering in which there is a small momentum transfer to the struck nucleon, thus lowering the observed cross section at forward angles. Attempts to estimate this change theoretically [1–6] are in general agreement. However, these estimates are not sufficient to reproduce (p, p') data accurately.

Instead we will use an empirical interaction that starts with the interaction of von Geramb [1]. The strength of the isoscalar central and spin-orbit parts are adjusted, and a density dependence is added in an amount chosen to match a body of (p, p') inelastic scattering data on $N = Z$ nuclei. In the work by Seifert *et al.* [16], a parametrization (PH3) was obtained for 200 MeV protons on ^{16}O and ^{40}Ca. By applying this interaction here, we will be testing it for masses lighter than those used to determine the parametrization.

We have chosen to first examine the 4^+ transition to the state at 6.02 MeV since this transition has the most collective properties of any of the ^{10}B transitions and is therefore most like the states used to determine the empirical interaction. In Fig. 5, we show calculations made with LEA using the free von Geramb interaction (dashed lines) and the density-dependent empirical interaction of Seifert (solid lines). As expected, the cross section is reduced at forward angles, bringing the calculation into accord with the data there. The size of the oscillation pattern in the analyzing power is increased and moved slightly forward in angle. Both these changes are helpful for the agreement with the data. In the work of Seifert, the data for ^{16}O and ^{40}Ca scattering did not extend to angles larger than about 60°, so our comparison beyond those angles is an extrapolation. At these larger angles, the agreement with the calculations is clearly worse. The calculated cross section falls too rapidly with angle, and the oscillation pattern in the analyzing power begins to get out of phase with that in the data. Otherwise, these calculations appear to be successful. The density-dependent feature of the effective interaction is needed for a good description of the data. These results also depend on the quality of the reproduction of the form factor [the same normalization is used for both (e, e') and (p, p') cases] and the treatment of the optical model distortions.

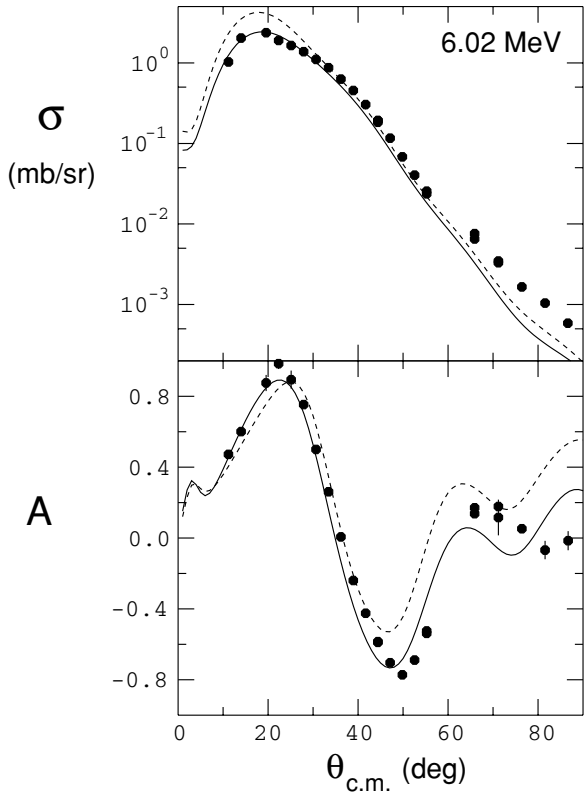

FIG. 5. Measurements of the cross section and analyzing power angular distributions for the 4^+ transition to the state at 6.02 MeV in ^{10}B. Dashed (solid) curves are calculations with a free (density-dependent) effective interaction [16].

The empirical interaction of Seifert has been tested against measurements of polarization transfer [18] with considerable success for collective, natural parity transitions. There it was noted that for small ΔL transfer, the polarization transfer observables also tended to obey the relationships required for elastic proton scattering from a spin-0 target. These relationships are illustrated in Figs. 6 and 7 by overlapping data points that are expected to be the same. For the in-plane polarization transfer measurements, the resolution at large scattering angles was not sufficient to resolve this state from its neighbors, and these data points have not been included in the figures. According to Liu *et al.* [18], the relationships $P = A$ and $D_{LS'} = -D_{SL'}$ are expected to be observed the best. The agreement between the two sets of data, and likewise between the two calculations, appears to be good and better than the agreement between data and calculation for any observable, even though this agreement also seems satisfactory. The relationships $D_{NN'} = 1$ and $D_{LL'} = D_{SS'}$ should be less well observed. In Fig. 7, the agreement with the latter relationship appears to be of high quality. However, $D_{NN'} < 1$ over most of the angular range, indicating significant contributions from spin-flip processes in this transition. For $D_{NN'}$ the agreement with the theory is still roughly satisfactory, indicating that the bulk of the spin-flip amplitude is included there, as opposed to the elastic scattering case. The good general agreement with other polarization observables tends to support the use of the empirical effective interaction for these transitions. This result

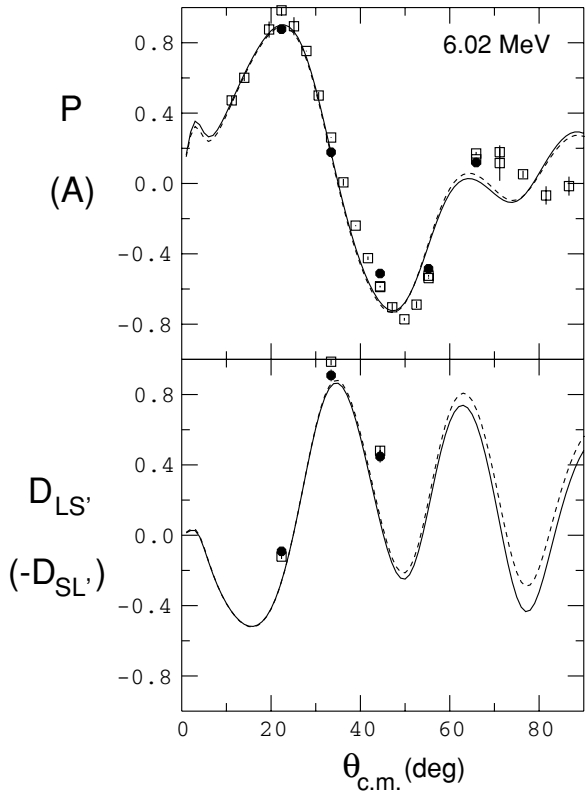

FIG. 6. Measurements of P and $D_{LS'}$ (solid points) along with A and $-D_{SL'}$ (open points) as a function of the center-of-mass scattering angle for the 4^+ transition to the state at 6.02 MeV in ^{10}B. The curves compare the empirical effective interaction with the data (solid lines with solid points, dashed lines with open points).

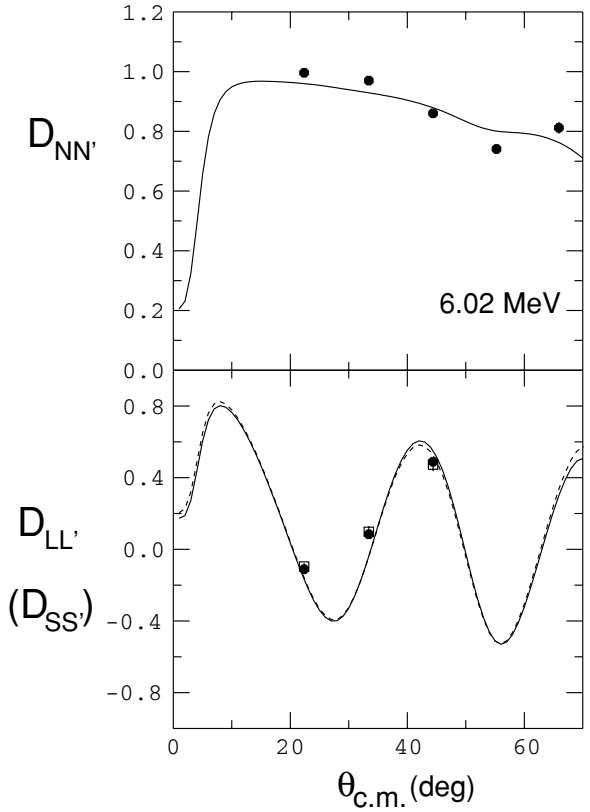

FIG. 7. Same as Fig. 6, but for $D_{NN'}$ and $D_{LL'}$ (solid points) along with D_{SS} (open points).

is in accord with the good agreement found in [18], and in fact extends that result to a larger range of angles and to a target mass lighter than the one on which the empirical interaction was based.

D. Comparisons with the other inelastic transitions

As seen in the last section, the calculations for the large collective 4^+ state at 6.02 MeV are generally successful. We would now like to turn to the comparison with the remaining natural parity transitions in ^{10}B. The 1^+, 2^+, and 3^+ states still have considerable collective character (mainly $\Delta L = 2$) but a much smaller cross section. In these cases, there is a relatively larger magnetic contribution, and we are likely to be sensitive to a greater degree of cancellation among the contributing particle-hole amplitudes. So the agreement with calculations may not be as good as noted for the 4^+ state. In addition, the 3^+ state at 4.77 MeV may contain a large $\Delta L = 0$ contribution not described by the particle-hole basis we are using. Agreement here may be the least satisfactory. In all of these calculations, only the density-dependent interaction of Seifert [16] will be used, since the discussion in the last section has shown it to be satisfactory for at least the collective parts of these transitions.

The cross-section data are shown in Fig. 8. Agreement forward of 60° seems generally satisfactory. At larger angles, the data are underestimated by the calculation, which is finally almost an order of magnitude too small. This difference is larger than it was for the 4^+ state. The only other systematic problem is a small tendency to overestimate the cross section in the region between 30° and 40°.

We show in Fig. 9 the angular distributions of A and P overlaid, and of $D_{LS'}$ and $-D_{SL'}$ overlaid. Good agreement is still obtained in the experiment for these strongly connected observables. So these transitions still follow the elastic scattering pattern. Likewise the density-dependent calculations for each member of the pairs are close. But there are now larger systematic disagreements between the calculations and the data. In particular, the first positive lobe of $D_{LS'}$ or $-D_{SL'}$ is underestimated, and the second positive lobe is too large. At the larger angles there are also problems with A and P, even though things are generally better forward of 60°. The differences in the size of the oscillation pattern in the angular distributions of A and P for the two 1^+ states (0.72 and 2.15 MeV) is well reproduced, suggesting that the structure difference between these two transitions is well described by the present set of shell-model matrix elements. There seems to be a special issue with the 2^+ transition at 3.59 MeV, since A and P are also not well reproduced even at forward angles. The structure information here may be faulty.

Looking at a similar comparison in Fig. 10, we see that the data again support the rule that $D_{LL'} = D_{SS'}$, but now in this weaker case the calculation does not. The comparison for $D_{NN'}$ between data and calculation suggests that there is now

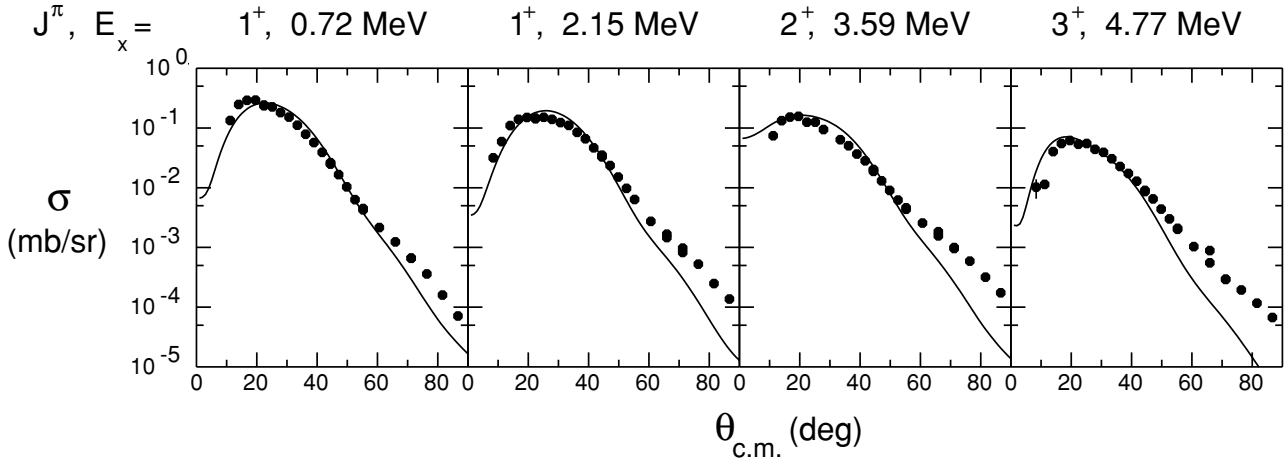

FIG. 8. Measurements of the cross section angular distribution for the 1^+ state at 0.72 MeV, the 1^+ state at 2.15 MeV, the 2^+ state at 3.59 MeV, and the 3^+ state at 4.77 MeV. The curves show the density-dependent effective interaction of Seifert [16].

less spin flip in the reaction than the calculation would suggest. Taken together, these data point to more collective behavior in these transitions than is contained in the shell-model structure calculations.

In a qualitative way, the calculations here describe the trends in the data, including the phase of the diffractive oscillations in the spin dependence. We have examined things in a hierarchy in which observables that ought to appear in pairs in strongly collective transitions are plotted together. We looked first at those pairings that ought to be the best satisfied. This procedure seems to suggest that these states in ^{10}B are highly collective. That the calculations do not follow (whereas they do for the 4^+ state at 6.02 MeV) would suggest that there are noncollective contributions to the structure we have put into

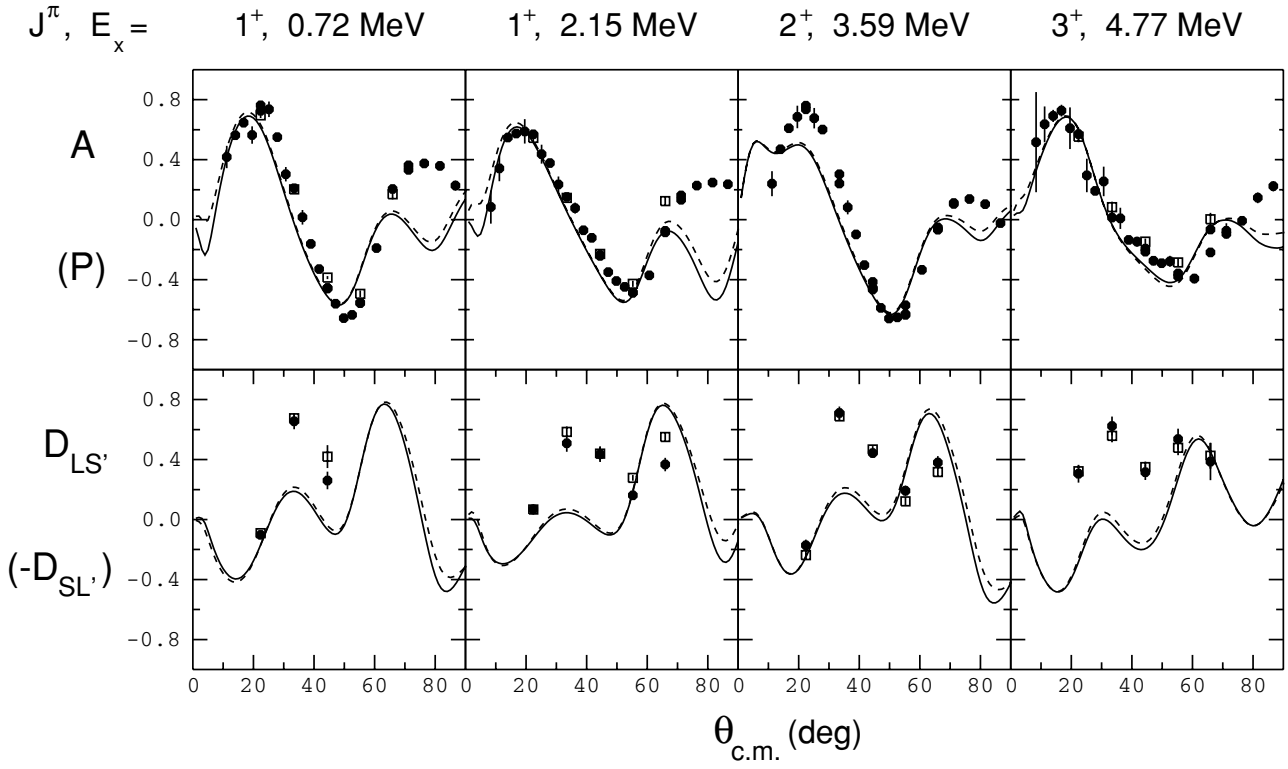

FIG. 9. Measurements of A (solid points in upper panel), P (open squares in upper panels), $D_{LS'}$ (solid points in lower panels), and $-D_{SL'}$ (open squares on lower panels) as a function of the scattering angle. Calculations using a density-dependent interaction are shown as solid curves for A and $D_{LS'}$, and as dashed curves for P and $D_{SL'}$. Excitation energies for the four transitions appear at the top of each column.

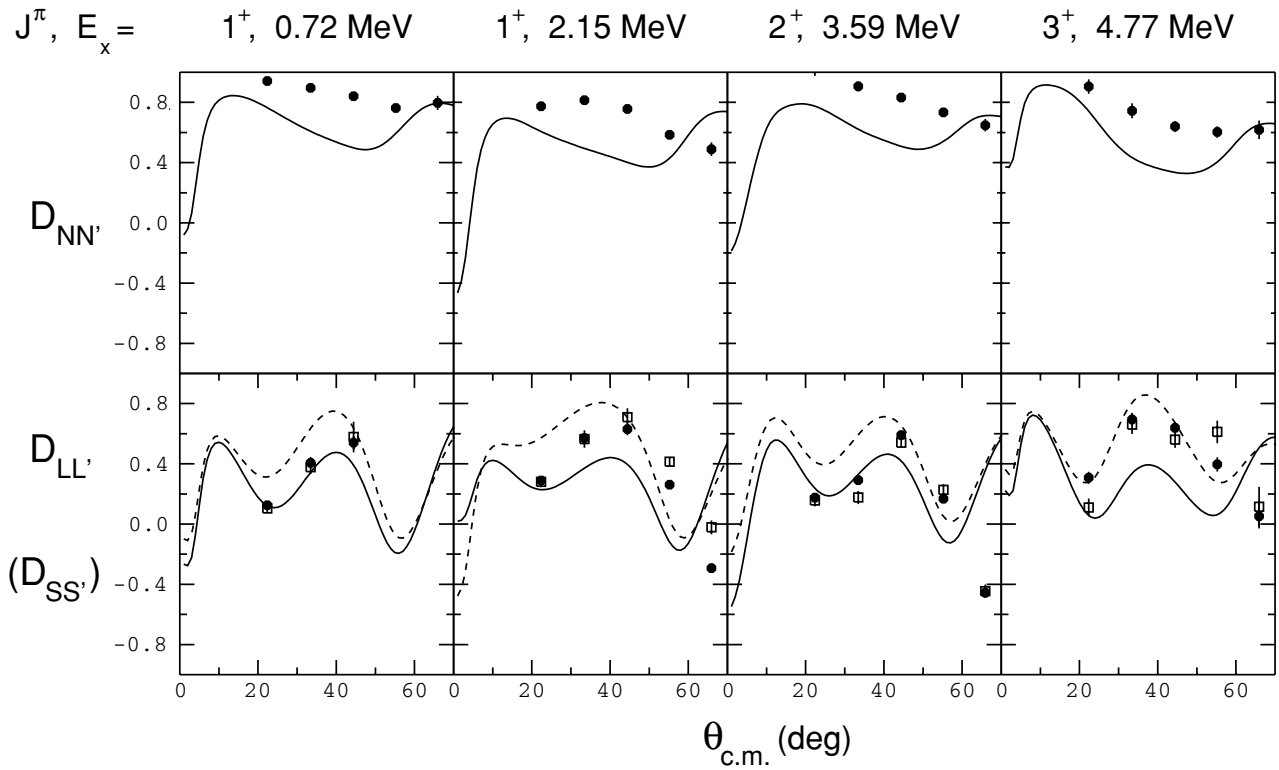

FIG. 10. Measurements of $D_{NN'}$ (top panels), $D_{LL'}$ (solid points in lower panels), and $D_{SS'}$ (dashed points in lower panels) as a function of the scattering angle. Calculations using a density-dependent interaction are shown as solid curves for $D_{NN'}$ and $D_{LL'}$, and as dashed lines for $D_{SS'}$. Excitation energies for the four transitions appear at the top of each column.

these calculations that play a much reduced role in the real measurements.

IV. CONCLUSIONS

We reported measurements of the cross section, analyzing power, induced polarization, and a complete set of polarization transfer coefficients for the natural parity transitions in ^{10}B$(\vec{p}, \vec{p}')^{10}$B leading to discrete final states. We then included as much information as possible on the structure of these transitions and worked with an empirical effective interaction in an effort to come as close as we could to these data with DWIA calculations. The nonvanishing spin of the ^{10}B ground state allowed multiple values of J transfer, and the most important of these possibilities were incorporated through a set of particle-hole matrix elements built on the p shell. While we started with shell-model values for these matrix elements, we changed the strength of the $L = 2$ part to match inelastic electron scattering data. This, along with the adjustment of the length parameter in the harmonic oscillator wave functions, allowed us to begin with a set of particle-hole matrix elements that agreed with the electron scattering data. We included the self-coupling in the ^{10}B ground state and coupling to the large 4^+ state at 6.02 MeV in our reaction calculations.

The polarization measurements exhibited an internal consistency that is similar to the rules for scattering a spin-1/2 projectile elastically from a spin-0 target, despite the presence of multiple values of J transfer. These included $A = P$, $D_{SL'} = -D_{LS'}$, and $D_{LL'} = D_{SS'}$. Deviations of $D_{NN'}$ from unity reflect the spin-flip contributions to the scattering.

Agreement between the data and the DWIA calculations was good, particularly in the angular range inside 60° where the parametrization of the effective interaction had been matched to collective transition data on heavier nuclei. This supports the wider application of such interactions as adequate descriptions of the effective interactions regardless of the mass of the target. The quality of the agreement with the polarization observables was best for A, P, $D_{SL'}$, and $D_{LS'}$ and not as good for $D_{NN'}$, $D_{SS'}$, and $D_{LL'}$. The agreement was overall the best for the 4^+ transition at 6.02 MeV, suggesting that the calculations work best for the more collective transitions. The least well described were the polarization observables for elastic scattering. There the analyzing power deviated from the data past 30°, and $D_{NN'}$ did not match the large amount of spin flip demonstrated by the data. In general, the calculations led to a successful understanding of these transitions, demonstrating the need to maintain consistency with the electron scattering data and to include strong channel-coupling effects.

ACKNOWLEDGMENTS

This work was supported by NSF Grants PHY-9602872 and PHY-0100348. E.J.S. acknowledges useful conversations with John Millener.

[1] H. V. von Geramb, in *The Interaction Between Medium Energy Nucleons in Nuclei – 1982*, AIP Conf. Proc. 97 (AIP, New York, 1983), p. 44.
[2] L. Rikus, K. Nakano, and H. V. von Geramb, Nucl. Phys. **A414**, 413 (1984).
[3] K. Nakayama and W. G. Love, Phys. Rev. C **38**, 51 (1988).
[4] L. Ray, Phys. Rev. C **41**, 2816 (1990).
[5] K. Amos, P. J. Dortmans, H. V. von Geramb, S. Karatiglidis, and J. Raynal, Adv. Nucl. Phys. **25**, 275 (2000).
[6] E. J. Stephenson, R. C. Johnson, and F. Sammarruca, Phys. Rev. C **71**, 014612 (2005).
[7] R. Machleidt, Adv. Nucl. Phys. **19**, 189 (1989).
[8] M. R. Anatasio, L. S. Celenza, W. S. Pong, and C. M. Shakin, Phys. Rep. **100**, 327 (1983).
[9] R. Brockmann and R. Machleidt, Phys. Lett. **B149**, 283 (1984); Phys. Rev. C. **42**, 1965 (1990)
[10] C. J. Horowitz and B. D. Serot, Phys. Lett. **B137**, 287 (1984); Nucl. Phys. **A464**, 613 (1987)
[11] B. ter Harr and R. Malfleit, Phys. Rep. **149**, 207 (1987).
[12] F. Sammarruca, E. J. Stephenson, and K. Jiang, Phys. Rev. C **60**, 064610 (1999).
[13] F. Sammarruca, E. J. Stephenson, K. Jiang, J. Liu, C. Olmer, A. K. Opper, and S. W. Wissink, Phys. Rev. C **61**, 014309 (1999).
[14] J. J. Kelly *et al*., Phys. Rev. C **39**, 1222 (1989).
[15] James J. Kelly, Phys. Rev. C **39**, 2120 (1989).
[16] H. Seifert *et al*., Phys. Rev. C **47**, 1615 (1993) and references therein.
[17] F. Sammarruca and E. J. Stephenson, Phys. Rev. C **64**, 034006 (2001).
[18] Jian Liu, E. J. Stephenson, A. D. Bacher, S. M. Bowyer, S. Chang, C. Olmer, S. P. Wells, S. W. Wissink, and J. Lisantti, Phys. Rev. C **53**, 1711 (1996).
[19] James J. Kelly, program LEA (May 1995 version), private communication.
[20] J. J. Kelly, Phys. Rev. C **46**, 711 (1992).
[21] B. S. Flanders *et al*., Phys. Rev. C **43**, 2103 (1991).
[22] H. Baghaei *et al*., Phys. Rev. Lett. **69**, 2054 (1992).
[23] W. Haeberli, Annu. Rev. Nucl. Sci. **17**, 373 (1967).
[24] P. Schwandt, T. B. Clegg, and W. Haeberli, Nucl. Phys. **A163**, 432 (1971).
[25] S. W. Wissink *et al*., IUCF Sci. Tech. Rep., 1989–1990 (unpublished), p. 180.
[26] S. P. Wells *et al*., Nucl. Instrum. Methods A **325**, 205 (1993).
[27] W. Bertozzi *et al*., Nucl. Instrum. Methods **141**, 457 (1977).
[28] A. H. Walenta *et al*., Nucl. Instrum. Methods **111**, 467 (1973).
[29] A. Cichocki, J. Dubach, R. S. Hicks, G. A. Peterson, C. W. de Jager, H. de Vries, N. Kalantar-Nayestanaki, and T. Sato, Phys. Rev. C **51**, 2406 (1995).
[30] T. Stovall, J. Goldemberg, and D. B. Isabelle, Nucl. Phys. **86**, 225 (1966).
[31] R. S. Hicks, J. Button-Shafer, B. Debebe, J. Dubach, A. Hotta, R. L. Huffman, R. A. Lindgren, G. A. Peterson, R. P. Singhal, and C. W. de Jager, Phys. Rev. Lett. **60**, 905 (1988).
[32] T.-S. H. Lee and D. Kurath, Phys. Rev. C **21**, 293 (1980).
[33] S. Cohen and D. Kurath, Nucl. Phys. **73**, 1 (1965).
[34] B. A. Brown *et al*., The Oxford-Buenos Aires-MSU shell model program OXBASH, Michigan State University Cyclotron Laboratory Report No. 524 (1986).
[35] D. J. Millener and D. Kurath, Nucl. Phys. **A255**, 315 (1975).
[36] P. R. Lewis, G. G. Shute, B. M. Spicer, R. S. Henderson, R. Abegg, D. Frekers, O. Häusser, K. P. Jackson, C. A. Miller, and S. Yen, Nucl. Phys. **A532**, 583 (1991).
[37] H. O. Meyer, P. Schwandt, G. L. Moake, and P. P. Singh, Phys. Rev. C **23**, 616 (1981).
[38] J. R. Comfort, Comput. Phys. Commun. **16**, 35 (1978).